ACS Chemical Neuroscience

Research Article

pubs.acs.org/chemneuro

Synthesis and Preliminary Evaluation of *N*-(16-^{18}F-Fluorohexadecanoyl)ethanolamine (^{18}F-FHEA) as a PET Probe of *N*-Acylethanolamine Metabolism in Mouse Brain

Mukesh K. Pandey,[†,§] Timothy R. DeGrado,*[,†,§] Kun Qian,[∥] Mark S. Jacobson,[†] Clinton E. Hagen,[‡] Richard I. Duclos, Jr.,[∥] and S. John Gatley*[,∥]

[†]Division of Nuclear Medicine, Department of Radiology, and [‡]Division of Biomedical Statistics and Informatics, Mayo Clinic, Rochester, Minnesota 55905, United States

[§]Brigham and Women's Hospital, Harvard Medical School, Boston, Massachusetts 02115, United States

[∥]Department of Pharmaceutical Sciences, Northeastern University, Boston, Massachusetts 02115, United States

Supporting Information

ABSTRACT: *N*-Acylethanolamines are lipid signaling molecules found throughout the plant and animal kingdoms. The best-known mammalian compound of this class is anandamide, *N*-arachidonoylethanolamine, one of the endogenous ligands of cannabinoid CB1 and CB2 receptors. Signaling by *N*-acylethanolamines is terminated by release of the ethanolamine moiety by hydrolyzing enzymes such as fatty acid amide hydrolase (FAAH) and *N*-acylethanolamine-hydrolyzing amidase (NAAA). Herein, we report the design and synthesis of *N*-(16-^{18}F-fluorohexadecanoyl)-ethanolamine (^{18}F-FHEA) as a positron emission tomography (PET) probe for imaging the activity of *N*-acylethanolamine hydrolyzing enzymes in the brain. Following intravenous administration of ^{18}F-FHEA in Swiss Webster mice, ^{18}F-FHEA was extracted from blood by the brain and underwent hydrolysis at the amide bond and incorporation of the resultant ^{18}F-fluorofatty acid into complex lipid pools. Pretreatment of mice with the FAAH inhibitor URB-597 (1 mg/kg IP) resulted in significantly slower ^{18}F-FHEA incorporation into lipid pools, but overall ^{18}F concentrations in brain regions were not altered. Likewise, pretreatment with a NAAA inhibitor, (*S*)-*N*-(2-oxo-3-oxytanyl)biphenyl-4-carboxamide (30 mg/kg IV), did not significantly affect the uptake of ^{18}F-FHEA in the brain. Although evidence was found that ^{18}F-FHEA behaves as a substrate of FAAH in the brain, the lack of sensitivity of brain uptake kinetics to FAAH inhibition discourages its use as a metabolically trapped PET probe of *N*-acylethanolamine hydrolyzing enzyme activity.

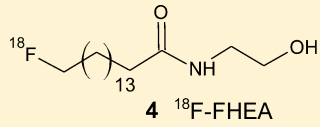

4 ^{18}F-FHEA

KEYWORDS: *Endocannabinoids, N-acylethanolamines, N-(16-^{18}F-fluorohexadecanoyl)ethanolamine, ^{18}F-FHEA, PET*

N-Acylethanolamines, including *N*-palmitoylethanolamine and *N*-arachidonoylethanolamine (anandamide), have diverse actions at cannabinoid receptors and other endocannabinoid systems. Their actions are terminated by fatty acid amide hydrolase (FAAH) and/or *N*-acylethanolamine-hydrolyzing amidase (NAAA). Changes in *N*-acylethanolamine levels and/or cannabinoid receptor (CB1/2) expression have been reported in many pathological states.[1,2] The three major areas of endocannabinoid actions are stress recovery and behavior,[1,2] energy balance through food regulation,[3] and immune and inflammatory regulation.[4] Endocannabinoid signaling may be dysregulated in a number of mental disorders, including bipolar disorder, depression, anxiety disorders, and dysfunctional response to chronic stress.[1,2,5−8] A noninvasive imaging method for monitoring *N*-acylethanolamine kinetics in the brain could have potential utility to help in our understanding of endocannabinoid processing. Of particular interest would be the potential for mapping of activity of *N*-acylethanolamine hydrolyzing enzymes (FAAH and NAAA) in various psychiatric and neurological disorders.

Wyffels et al.[9] reported development of single photon emission computed tomography (SPECT) imaging agents for evaluation of FAAH activity, whereby ^{123}I was substituted for the ethanolic hydroxyl group on *N*-linoleoylethanoamine and *N*-arachidonoylethanolamine (anandamide). The highest uptake values for ^{123}I-labeled *N*-(2-iodoethyl)linoleoylamide and *N*-(2-iodoethyl)arachidonylamide were reported to be 1.23% ID/g at 3 min and 0.58%ID/g at 10 min post-injection in brain, respectively, but no retention of radioactivity was observed.[9] These authors explained the lower uptake and poor retention in brain due to instability of the tracer. The same group modified their molecules to develop a series of compounds as aryl anandamide analogues.[10] Among those, two of them were labeled with ^{11}C to achieve positron emission tomography (PET) imaging agents.[10] On careful analysis, it is noted that these authors have again replaced the hydroxyl group of the ethanolamine component with substituents to develop aryl analogues of *N*-linoleoylethanoamine and *N*-arachidonoylethanolamine (anandamide). The highest brain uptake value was 1.44 ± 0.02%ID/g at 1 min post-injection, with continuous washout over time.[10] Furthermore, Wyffels et al.[11] labeled an

Received: December 4, 2013
Revised: July 8, 2014
Published: July 8, 2014

ACS Publications © 2014 American Chemical Society

Scheme 1. Synthesis of *N*-(16-^{18}F-Fluorohexadecanoyl)ethanolamine (^{18}F-FHEA)[a]

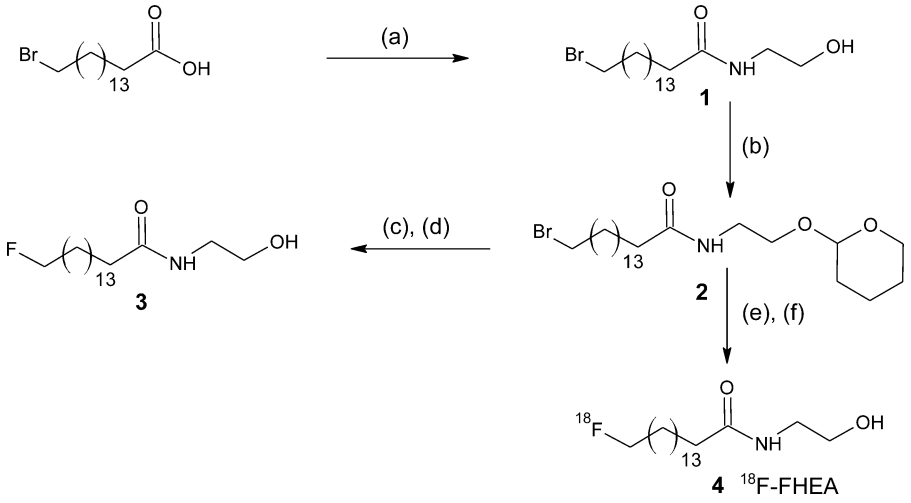

[a](a) Methyl chloroformate, ethanolamine, triethylamine, dichloromethane, 0 °C to RT; (b) 3,4-dihydro-2*H*-pyran, *p*-toluenesulfonic acid, dichloromethane, 12 h; (c) tetra-*n*-butylammonium fluoride, tetrahydrofuran; (d) aq methanol, *p*-toluenesulfonic acid; (e) K2.2.2, K^{18}F, K_2CO_3, microwave; (f) 15% trifluoroacetic acid solution, microwave.

analogue of the FAAH inhibitor URB-597 to map FAAH activity but the compound suffered extremely poor retention in brain. On the other hand, Glaser et al.[12] using ^{3}H-labeled anandamide found a brain uptake of 2.38 ± 0.22%ID at 5 min with retention in overall activity (both unmetabolized and metabolized) over time, indicating the importance of labeling position on the resulting brain kinetics following radiolabeled *N*-acylethanolamine hydrolysis.[12] In contrast to the work of Wyffels and co-workers[9,10] that labeled the ethanolamine component, we anticipated that labeling of the fatty acyl component would increase brain retention due to incorporation of the liberated fatty acid into various complex lipid pools. To support this notion, a different analogue of URB-597, [^{11}C]CURB, was developed by Wilson et al.,[13] which was labeled in a different position from that of Wyffels et al.[11] [^{11}C]CURB showed excellent preclinical in vivo results and is currently in human trials as [^{11}C]CURB.[13] [^{11}C]CURB is thought to be useful to measure the overall expression of FAAH in brain, as its metabolism by NAAA is relatively insignificant.

In the present approach, we anticipated that a radiotracer based on a close structural analogue of *N*-palmitoylethanolamine would be a substrate for both FAAH and NAAA.[14−17] FAAH has been studied in great detail,[1,18−20] but NAAA is relatively poorly understood.[15,16] NAAA was first reported in 1999, but in recent years it is being seen as an important enzyme in *N*-acylethanolamine metabolism.[15,16] NAAA is a lysosomal enzyme and shows highest activity at pH 4.5−5.0, whereas FAAH is a membrane-bound protein and exhibits highest activity at pH 8.5−10.[15] The Michaelis constant (K_m) for *N*-palmitoylethanolamine (PEA) against targeting enzymes FAAH and NAAA is 1.5 and 97 μM, respectively.[21,22]

We have previously conducted autoradiographic studies in mouse brain using ^{3}H-arachidonoylethanolamine (anandamide), and shown that regional disposition of label reflects incorporation into phospholipids of arachidonic acid liberated by FAAH.[12] To translate this methodology to PET, we have prepared and evaluated *N*-(16-^{18}F-fluorohexadecanoyl)-ethanolamine (^{18}F-FHEA), a structurally simpler compound than anandamide. While previous biological data on the nonradioactive form of FHEA itself is lacking, *N*-hexadecanoylethanolamine (palmitoylethanolamine) is a well-known FAAH substrate.[23,24] It has a very low affinity for cannabinoid receptors compared with anandamide, but higher affinity for peroxisome proliferator-activated receptor alpha (PPAR-alpha).[25,26] It possesses analgesic properties and is consumed as a "nutraceutical" for pain relief. In this study, we report on the radiosynthesis of ^{18}F-FHEA and initial brain uptake, biodistribution and metabolite analysis studies in mice.

RESULTS

Synthesis of ^{18}F-FHEA. Scheme 1 describes the synthesis of ^{18}F-FHEA (**4**). To synthesize the labeling precursor for ^{18}F-FHEA, 16-bromohexadecanoic acid was activated using methyl chloroformate and then reacted with ethanolamine in the presence of triethylamine to get *N*-(16-bromohexadecanoyl)-ethanolamine (**1**).[27] The obtained bromo-*N*-acylethanolamine **1** was treated with 3,4-dihydro-2*H*-pyran in the presence of *p*-toluenesulfonic acid in dichloromethane to obtain 16-bromo-*N*-[2[(tetrahydro-2*H*-pyran-2-yl)oxy]ethyl]hexadecanoylamide (**2**) as precursor for radiofluorination. The compound **2** served as precursor for radiofluorination. Before radiofluorination, compound **2** was treated with tetra-*n*-butylammonium fluoride in acetonitrile followed by deprotection using *p*-toluenesulfonic acid to obtain nonradioactive ^{19}F-FHEA (**3**) as a reference standard for HPLC.

The radiofluorination of the 16-bromo-*N*-[2[(tetrahydro-2*H*-pyran-2-yl)oxy]ethyl]hexadecanoylamide (**2**) using cyclotron-produced K^{18}F was carried out under microwave heating at 80 °C, 10 min as described previously.[28,29] Our recent use of a microwave reactor in nucleophilic radiofluorination of fatty acids[28,29] showed enhanced product yield with significant reduction in reaction time and side products.[29] Structural similarity of FHEA to those of the fatty acids gave us confidence on the application of radiofluorination of FHEA by incorporating a PETWave microwave reactor (CEM Corporation, Mathews NC) into a TRACERlab FXN Pro (GE HealthCare, Waukesha WI) radiosynthesis module during productions of ^{18}F-FHEA. Radiofluorination proceeded efficiently, with >90% incorporation of ^{18}F-fluoride into the corresponding amide. ^{18}F-Fluoro-*N*-[2[(tetrahydro-2*H*-pyran-

dx.doi.org/10.1021/cn400214j | ACS Chem. Neurosci. 2014, 5, 793−802

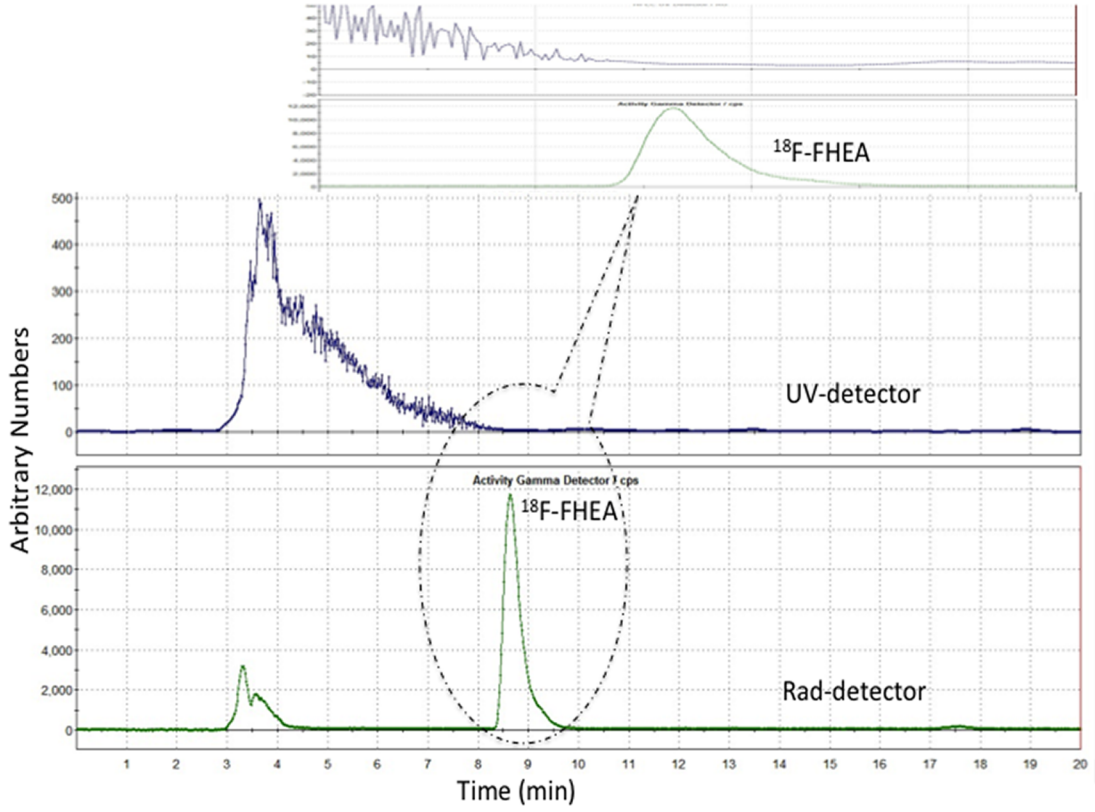

Figure 1. Preparative HPLC chromatogram of ^{18}F-FHEA.

2-yl)oxy]ethyl]hexadecanoylamide was quantitatively hydrolyzed by addition of 0.45 mL of 15% TFA (trifluoroacetic acid) aqueous solution and microwave heating (60 °C) for 5 min. The deprotected ^{18}F-FHEA product **4** was purified by semipreparative C-18 HPLC (80:20 ACN/H_2O, t_R = 7.3 min). Overall radiochemical yields after semipreparative HPLC isolation was in the range 12−21% decay-corrected. Radiochemical purity of the product (**4**) was >99% by radio-HPLC (Figure 1). The specific activity was estimated by measuring the minimum detection limit for nonradioactive FHEA as 5.2 μg using the preparative HPLC system. Based on this finding, we estimated the specific activity of ^{18}F-FHEA to be in the range of 1.4−5.1 Ci/μmol. The product was formulated in saline solution and passed through a sterile filter before administration to mice by tail-vein injection.

Synthesis of Nonradioactive Standards. The details for the synthesis of nonradioactive standards are described in the Supporting Information (Scheme SS1). The synthesized nonradioactive standards were utilized to identify possible labeled metabolites by HPLC/TLC. A separate synthetic route (Scheme SS1, Supporting Information) starting with omega hydroxy fatty ester was utilized because of two reasons: (1) to avoid use of the bromo precursor **2** for multiple step synthesis of nonradioactive standards and (2) to avoid the poor product yield of bromo to fluoro conversion.

Synthesis of NAAA Inhibitor. Due to the absence of a commercial source for a potent and selective NAAA inhibitor, we chose (*S*)-*N*-(2-oxo-3-oxytanyl)biphenyl-4-carboxamide (Compound 7h) as one of the most potent NAAA inhibitor reported in the literature with IC_{50} value 115 ± 13 nm (Scheme 2).[30] A multistep synthesis and characterization was carried out following the literature method described by Solorzano et al.[30] The synthesized NAAA inhibitor was formulated in dimethyl

Scheme 2. Chemical Structures of FAAH and NAAA Inhibitors

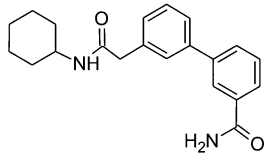

FAAH inhibitor URB597

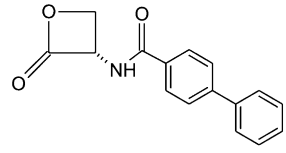

NAAA inhibitor- Compound 7h*

* Ref. 28, 29

sulfoxide/Cremophor/0.9% saline (20 μL/30 μL/150 μL) solutions. Each injection was 200 μL having 0.75 mg of NAAA inhibitor (20 mg/kg, Compound 7h). Although the same authors reported limited stability of Compound 7h in buffer (half-life of 12.6 ± 1.4 min at pH 7.4),[31] we reasoned that there would be sufficient stability to allow inhibition of NAAA following intravenous administration in mice.

Biodistribution and Brain Uptake Studies in Mice with and without FAAH Inhibitor. ^{18}F-FHEA's role in lipid signaling pathways and imaging potential were evaluated by measuring biodistribution and brain uptake in Swiss Webster mice. ^{18}F-FHEA uptake in brain regions as well as blood and urine were evaluated at five different time points between 1 and 60 min (Tables 1−3). Regional brain uptake was fairly constant from 1 to 60 min with the exception of the cortex, which differed over time ($p < 0.05$). The uptake differed across brain regions at each time point (Table 1). Urinal clearance was evident over time, while ^{18}F-FHEA in blood and whole brain remained (Table 2). Standardized uptake across all brain regions was statistically different at each time point. Concentrations in the hypothalamus ($p < 0.002$), thalamus (p

dx.doi.org/10.1021/cn400214j | ACS Chem. Neurosci. 2014, 5, 793−802

Table 1. Biodistribution (% ID/g) of ^{18}F-FHEA in Swiss Webster Mice Following Intravenous Administration[a]

tissue	1 min	5 min	15 min	30 min	60 min	*p*-value[b]
hypothalamus	2.88 ± 0.63	3.05 ± 0.47	2.04 ± 0.30[e]	2.13 ± 0.07	2.83 ± 0.90[e]	0.1276
ophthalmic tubules	3.21 ± 0.59	3.05 ± 0.43	2.54 ± 0.14[e]	2.55 ± 0.28	3.50 ± 1.33[e]	0.2261
hippocampus	2.55 ± 0.65[e]	2.52 ± 0.33	2.18 ± 0.03[e]	2.15 ± 0.35	3.09 ± 0.094[e]	0.3300
striatum	3.17 ± 0.55	2.92 ± 0.47	2.57 ± 0.23[e]	2.54 ± 0.35	3.78 ± 0.88[e]	0.1050
cerebellum	3.57 ± 0.69	3.42 ± 0.50	2.98 ± 0.22[e]	3.01 ± 0.37	4.21 ± 1.23[e]	0.1207
brain stem	3.63 ± 0.72	3.58 ± 0.56	2.95 ± 0.18[e]	2.66 ± 0.29	3.78 ± 1.18[e]	0.1011
cortex	3.61 ± 0.57	3.39 ± 0.52	2.87 ± 0.16[e]	2.90 ± 0.45	4.32 ± 1.37[e]	0.0455[d]
thalamus	3.30 ± 0.64	3.53 ± 0.47	2.64 ± 0.38[e]	2.45 ± 0.36	3.60 ± 0.99[e]	0.0697
whole brain	3.16 ± 0.76	3.14 ± 0.40	2.68 ± 0.22[e]	2.64 ± 0.30	3.69 ± 1.08[e]	0.2172
p-value[c]	<0.0001[d]	<0.0001[d]	<0.0001[d]	<0.0001[d]	<0.0001[d]	**overall model** <0.0001[d]

[a]Values are listed as mean ± standard deviation. There were 4 measurements for each time by body region category unless otherwise indicated. A random effects ANOVA was used to account for the repeated measurements (a measurement for each region) on each animal. Time was modeled as a between subject factor. There was a significant region by time interaction. [b]*p*-Values represent tests for differences in biodistribution across times. *p*-Values are not adjusted for multiple comparisons. [c]*p*-Values represent tests for differences in biodistribution across body regions. *p*-Values are not adjusted for multiple comparisons. [d]Statistically significant *p*-value. [e]$n = 3$.

Table 2. Comparison of Uptake (% ID/g) of ^{18}F-FHEA in Whole Brain, Blood, and Urine of the Swiss Webster Mice Following Intravenous Administration at Different Time Points[a]

tissue	1 min	5 min	15 min	30 min	60 min	*p*-value[b]
whole brain	3.16 ± 0.76	3.14 ± 0.40	2.68 ± 0.22[e]	2.64 ± 0.30	3.69 ± 1.08[e]	0.9997
blood	2.80 ± 0.77[e]	1.72 ± 0.20	1.43 ± 0.38[f]	2.29 ± 0.16	1.79 ± 0.16[e]	0.9994
urine	1.00 ± 1.95	29.83 ± 7.05	28.06 ± 1.59[f]	35.90 ± 12.44	43.60 ± 32.99[f]	<0.0001[d]
p-value[c]	0.8992	<0.0001[d]	0.0004[d]	<0.0001[d]	<0.0001[d]	**overall model** <0.0001[d]

[a]Values are listed as mean ± standard deviation. There were four measurements for each time by body region category unless otherwise indicated. A random effects ANOVA was used to account for the repeated measurements (a measurement for each region) on each animal. Time was modeled as a between subject factor. There was a significant region by time interaction. [b]*p*-Values represent tests for differences in biodistribution across times. *p*-Values are not adjusted for multiple comparisons. [c]*p*-Values represent tests for differences in biodistribution across body regions. *p*-Values are not adjusted for multiple comparisons. [d]Statistically significant *p*-value. [e]$n = 3$. [f]$n = 2$.

Table 3. Tissue/Whole Brain Ratios (T/WB) of uptake (% ID/g) of F-FHEA of the Swiss Webster Mice Following Intravenous Administration[a]

tissue	1 min	5 min	15 min[e]	30 min	60 min[e]	*p*-value[b]
hypothalamus	0.92 ± 0.08	0.97 ± 0.06	0.76 ± 0.06	0.81 ± 0.07	0.79 ± 0.27	0.0013[d]
ophthalmic tubules	1.03 ± 0.07	0.97 ± 0.06	0.95 ± 0.03	0.97 ± 0.04	0.93 ± 0.08	0.5597
hippocampus	0.75 ± 0.04[e]	0.80 ± 0.02	0.82 ± 0.05	0.81 ± 0.06	0.84 ± 0.01	0.9334
striatum	1.02 ± 0.14	0.93 ± 0.06	0.96 ± 0.03	0.96 ± 0.04	1.04 ± 0.06	0.2817
cerebellum	1.14 ± 0.07	1.09 ± 0.03	1.12 ± 0.01	1.14 ± 0.03	1.14 ± 0.03	0.8404
brain stem	1.16 ± 0.12	1.14 ± 0.06	1.10 ± 0.05	1.01 ± 0.02	1.02 ± 0.03	0.0219[d]
cortex	1.16 ± 0.10	1.08 ± 0.06	1.08 ± 0.07	1.09 ± 0.05	1.17 ± 0.10	0.3153
thalamus	1.05 ± 0.10	1.12 ± 0.04	0.99 ± 0.06	0.93 ± 0.07	0.98 ± 0.02	0.0059[d]
p-value[c]	<0.0001[d]	<0.0001[d]	<0.0001[d]	<0.0001[d]	<0.0001[d]	**overall model** <0.0001[d]

[a]Values are listed as mean ± standard deviation. There were four measurements for each time by body region category unless otherwise indicated. A random effects ANOVA was used to account for the repeated measurements (a measurement for each region) on each animal. Time was modeled as a between subject factor. There was a significant region by time interaction. [b]*p*-Values represent tests for differences in biodistribution across times. *p*-Values are not adjusted for multiple comparisons. [c]*p*-Values represent tests for differences in biodistribution across body regions. *p*-Values are not adjusted for multiple comparisons. [d]Statistically significant *p*-value. [e]$n = 3$.

< 0.006), and brain stem ($p < 0.03$) were different across time points (Table 3). The biodistribution data obtained at 30 min after intravenous administration of ^{18}F-FHEA are listed in Table 4. The effect of FAAH inhibitor on ^{18}F-FHEA uptake was evaluated by intraperitoneal administration of URB 597 (1 mg/kg) 60 min prior to the intravenous injection of ^{18}F-FHEA to the mice. Uptakes were examined by measuring percentage of injected dose per gram of the tissue (% ID/g) and standard uptake value (SUV). The biodistribution data showed that ^{18}F-FHEA was widely distributed throughout the body (Table 4). The only region that showed a significant effect of URB-597 was the bone: bone uptake in animals pretreated with URB-597 was significantly higher than that in controls (6.24 ± 11.30 SUV versus 0.62 ± 0.10, $p < 0.0001$). Typically, higher bone uptake of metabolizable ^{18}F-labeled radiotracers signifies higher metabolic release of free ^{18}F-fluoride.

To determine whether pretreatment with a FAAH-inhibitor altered the chemical form of ^{18}F in the brain, we conducted chloroform/methanol extractions (Folch-type)[28,32] of cerebellar tissue 5 min after administration of FHEA, followed by radio-TLC analysis of the chloroform fractions (Figure 2). There was no significant difference in the fraction of extracted ^{18}F-radioactivity found in the chloroform layer (80 ± 4% for controls, 86 ± 3% for URB-597 treated; $p = 0.07$, $n = 4$). The

dx.doi.org/10.1021/cn400214j | ACS Chem. Neurosci. 2014, 5, 793−802

Table 4. Uptake (% ID/g) and SUV of ^{18}F-FHEA in Swiss Webster Mice at 30 min Post-Injection[a]

tissue	%ID/g control mice	%ID/g URB treated Mice	%ID/g p-value[b]	SUV control mice	SUV URB treated mice	SUV p-value[b]
cortex	3.50 ± 0.82	2.89 ± 0.28	0.9039	0.90 ± 0.17	0.77 ± 0.10	0.9231
cerebellum	2.75 ± 1.73	2.68 ± 0.41	0.9899	0.70 ± 0.43	0.71 ± 0.08	0.9962
brain stem	3.04 ± 0.87	2.69 ± 0.42	0.9442	0.78 ± 0.20	0.71 ± 0.11	0.9595
thalamus	3.06 ± 0.63	2.68 ± 0.33	0.9401	0.79 ± 0.13	0.71 ± 0.08	0.9540
hypothalamus	2.85 ± 1.08	2.41 ± 0.29	0.9298	0.73 ± 0.24	0.64 ± 0.09	0.9468
olfactory tubercle	2.72 ± 0.61	2.60 ± 0.65	0.9809	0.70 ± 0.14	0.69 ± 0.19	0.9944
hippocampus	2.68 ± 0.72	2.16 ± 0.25	0.9176	0.69 ± 0.18	0.57 ± 0.08	0.9318
striatum	3.26 ± 0.79	2.45 ± 0.29	0.8710	0.84 ± 0.18	0.65 ± 0.10	0.8901
whole brain	2.83 ± 1.29	2.69 ± 0.20	0.9841	0.72 ± 0.30[d]	0.71 ± 0.06	0.9985
blood	2.32 ± 0.47	2.19 ± 0.31	0.9798	0.60 ± 0.12	0.58 ± 0.07	0.9876
urine	10.91 ± 4.78[d]	20.46 ± 17.99	0.0859	2.90 ± 1.26[d]	5.57 ± 5.01	0.0818
heart	5.19 ± 1.23	5.20 ± 1.87	0.9981	1.35 ± 0.32	1.37 ± 0.45	0.9865
lung	9.83 ± 3.84	5.13 ± 0.64[d]	0.3725	2.53 ± 0.90	1.33 ± 0.14[d]	0.4229
liver	15.07 ± 4.86	15.19 ± 1.86	0.9807	3.88 ± 1.07	4.04 ± 0.54	0.9119
spleen	2.94 ± 0.21	2.47 ± 0.22	0.9259	0.76 ± 0.03	0.66 ± 0.06	0.9386
kidney	12.89 ± 2.31	11.08 ± 1.64	0.7172	3.34 ± 0.45	2.93 ± 0.38	0.7728
testis	1.17 ± 0.27	0.80 ± 0.15	0.9418	0.30 ± 0.07	0.21 ± 0.05	0.9490
fat	3.14 ± 1.76	3.41 ± 1.74	0.9582	0.81 ± 0.43	0.91 ± 0.47	0.9421
bone	2.39 ± 0.48	22.56 ± 40.59	<0.0001[c]	0.62 ± 0.10	6.24 ± 11.30	<0.0001[c]
muscle	2.50 ± 0.40	2.74 ± 0.96	0.9621	0.65 ± 0.08	0.72 ± 0.23	0.9572
skin	1.29 ± 0.19	1.40 ± 0.22	0.9818	0.33 ± 0.04	0.37 ± 0.05	0.9785
overall model p-value		%ID/g URB < 0.0001[c]			SUV URB < 0.0001[c]	

[a]Values are listed as mean ± standard deviation. There were 4 measurements for each time by body region category unless otherwise indicated. [b]p-Value represents tests for differences in biodistribution across treatment groups. p-Values are not adjusted for multiple comparisons. [c]Statistically significant p-value. [d]n = 3.

chloroform fractions were subjected to silica gel TLC analysis using two different solvent systems to analyze both polar and nonpolar metabolites. The nonpolar solvent system comprised petroleum ether/diethyl ether/acetic acid (70:30:1, v/v), whereas the polar solvent system was made up of chloroform/methanol/ammonium hydroxide (60:30:1, v/v). In the nonpolar system, there was a large peak at the origin, and several smaller peaks, at Rf values of 0.16, 0.29, 0.36−0.37 (Figure 2a). On the basis of TLCs of nonradioactive standards and synthesized metabolites, the peaks were assigned as (1) polar lipid (PL) and FHEA, (2) diglyceride (DG), (3) fatty acid (FA), (4) triglyceride (TG), and (5) cholesterol ester (CE) (Figure 2a). In the polar solvent system, there was a small peak at the origin, and peaks at about 0.02, 0.05, 0.2, 0.25, 0.44−0.47, 0.83−0.86, and 0.97 Rf (Figure 2b). Based on reference standards, the metabolites 1−7 were assigned as (1) lysophosphatidyl choline (LPC) and lysophosphatidyl ethanolamine (LPE), (2) phosphatidyl choline (PC), (3) phosphatidyl ethanolamine (PE), (4) unknown (UNK), (5) fatty acid (FA), (6) FHEA, (7) diglyceride (DG) and triglyceride (TG) and cholesterol ester (CE) (Figure 2b). In the vehicle-treated animals, the peak at 0.05 Rf (PC) was most prominent, whereas in the FAAH inhibitor-treated animals nonmetabolized ^{18}F-FHEA was most prominent.

Biodistribution and Brain Uptake of *N*-(16-^{18}F-Fluorohexadecanoyl)ethanolamine (^{18}F-FHEA) in Swiss Webster Mice with and without NAAA Inhibitor. The effect of a NAAA inhibitor on ^{18}F-FHEA uptake was evaluated by intravenous administration of Compound 7h (30 mg/kg) 15 min prior to the retro-orbital administration of ^{18}F-FHEA to the mice. Uptake values at 30 min after ^{18}F-FHEA administration are presented in Table 5. The biodistribution data showed that ^{18}F-FHEA was widely distributed throughout the body (Table 5). The highest uptake was found in liver, followed by lung and kidney in both control and NAAA inhibitor treated mice group. Among brain regions, the highest uptake was found in cerebellum followed by brain stem and thalamus. Uptake levels across brain regions were found to be similar and not statistically different in both control and NAAA inhibitor treated mice (Table 5). The representative micro-PET images of ^{18}F-FHEA with and without NAAA inhibitor were acquired, and but no significant difference was noticed on treatment with NAAA inhibitor (Figure S6, Supporting Information).

Measurement of IC_{50} for Inhibition of Anandamide Hydrolysis in Mouse Brain Homogenate. Competitive inhibition measurements using unlabeled *N*-palmitoylethanolamine (PEA) and *N*-fluorohexadecanoylethanolamine (FHEA) with ^{14}C-labeled anandamide in mouse brain homogenates were performed. FHEA (IC_{50} = 220 ± 33 μM, n=5) showed more potent inhibition of anandamide hydrolysis than PEA (IC_{50} = 443 ± 45 μM, n=3) (p < 0.01).

DISCUSSION

We synthesized and evaluated the ^{18}F-labeled palmitoylethanolamine analogue ^{18}F-FHEA to understand its potential as a PET tracer for *N*-acylethanolamine metabolism catalyzed by FAAH and/or NAAA. Biodistribution (Tables 1−5) and PET imaging (Figure S6, Supporting Information) studies showed that ^{18}F-FHEA crossed the blood-brain barrier and distributed rather homogeneously throughout the mouse brain. However, no differences in either global brain concentration of ^{18}F or of uptake in individual brain regions were observed between control mice and those treated with a dose of the FAAH inhibitor URB-597 (Table 4) shown by previous workers to block FAAH.[33]

The analysis of radiolabeled lipophilic ^{18}F-FHEA metabolites in the cerebellum at 5 min post-administration showed a

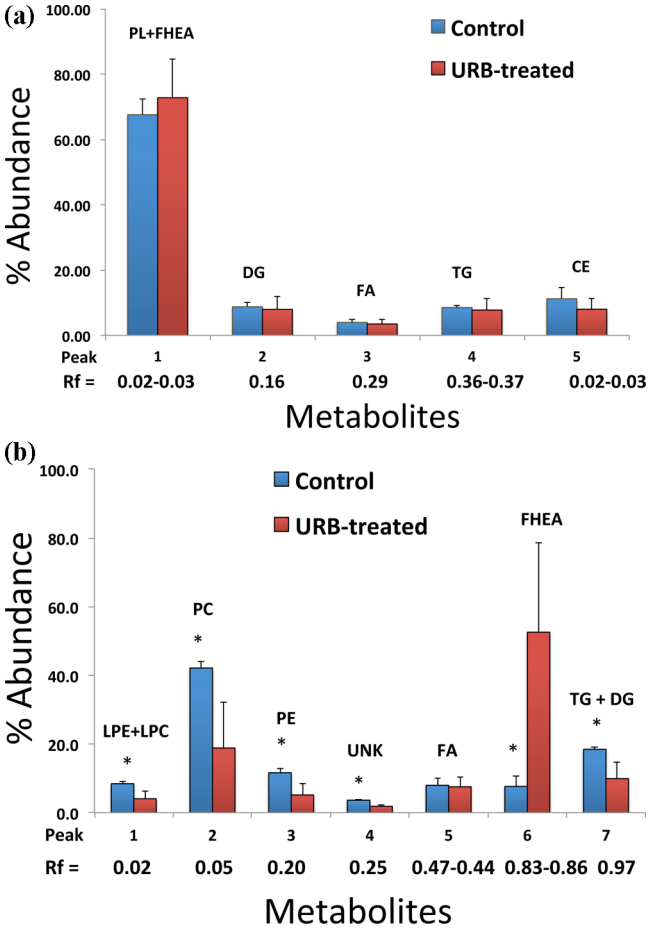

Figure 2. (a) Metabolite analysis of cerebellum by r-TLC measurement in a nonpolar solvent system (petroleum ether/diethyl ether/acetic acid, 70:30:1) after 5 min post-injection of *N*-(16-^{18}F-fluorohexadecanoyl)ethanolamine (3) to both control and URB 597 treated Swiss Webster mice. (PL, phospholipid; FHEA, fluorohexadecanoylethanolamine; MG, momoglyceride; DG, diglyceride; TG, triglyceride; CE, cholesterol ester.) (b) Metabolite analysis of cerebellum by r-TLC measurement in a polar solvent system (chloroform/methanol/ammonium hydroxide, 60:30:1) after 5 min post-injection of *N*-(16-^{18}F-fluorohexadecanoyl)ethanolamine (3) to both control and URB 597 treated Swiss Webster mice (n = 3, *P value <0.05, one tail Student's t test). (LPE, lysophosphatidylethanolamine; LPC, lysophosphatidylcholine; PC, phosphatidylcholine; PE, phosphatidylethanolamine; DG, diglyceride; UNK, unknown; FA, fatty acid; TG, triglyceride; CE, cholesterol ester.)

significantly reduced degree of metabolism of ^{18}F-FHEA to labeled phospholipids (Figure 2). Whereas in control mice the largest labeled lipid component was phosphatidyl choline, in URB-597 treated animals the most abundant labeled species was ^{18}F-FHEA, which increased from about 10% of the organic-soluble ^{18}F-radioactivity in controls to about 50% in animals treated with inhibitor. The degree of conversion to phospholipids of ^{18}F-FHEA in control brains was similar to the 60−70% of total tissue radiolabel seen at 5 min with [^{3}H]anandamide by Glaser et al.[12] Inhibition of incorporation of ^{18}F from ^{18}F-FHEA into complex lipids by URB-597 confirms the expectation that FHEA is a substrate for FAAH, but it is possible that other hydrolases contribute to its metabolism. For example, the study by Sun et al.[14] in macrophages observed the role of NAAA on *N*-acylethaloamine hydrolysis including anandamide and palmitoylethanolamine (PEA) as substrates. Accordingly, we also investigated ^{18}F-FHEA biodistribution with and without pretreatment with a known NAAA inhibitor. Since no inhibitors of NAAA are available commercially, we synthesized one of the most potent inhibitors described in the literature, "Compound **7h**" of Solorzano et al.[30] The potency of Compound 7h was established by in vitro inhibition of NAAA against PEA hydrolysis (IC_{50} = 115 nM);[30] however, data is lacking on the efficacy of Compound 7h as an in vivo inhibitor. In mice pretreated with Compound 7h, we did not measure any significant difference in uptake of ^{18}F-FHEA in brain and other organs at 30 min post-injection (Table 5). Since we have no firm evidence that NAAA was inhibited by Compound 7h at the levels administered in this study, these data remain inconclusive. However, the predominance of radioactivity in the form of nonmetabolized ^{18}F-FHEA in the cerebellum after specific FAAH inhibition by URB-597 argues that NAAA plays a relatively minor role in ^{18}F-FHEA metabolism in brain. Indeed, others have measured relatively low levels of NAAA in mouse brain.[34]

The finding that URB-597 did not significantly alter the brain regional concentration of ^{18}F-radioactivity after administration of FHEA, in spite of the fact that the lipid metabolites of ^{18}F-FHEA were dramatically changed, requires explanation. The transfer of ^{18}F-FHEA between blood and brain appears to be nearly unidirectional, so that while ^{18}F-FHEA can undergo rapid metabolism within the brain, unmetabolized ^{18}F-FHEA is also retained over the 30−60 min time period of our biodistribution measurements. Reasons for this are presently unclear, but one possibility is that ^{18}F-FHEA is retained in brain tissue by fatty acid binding proteins.[35,36]

An alternative approach to imaging FAAH, using high affinity binding radioligands such as ^{11}C-CURB and related ^{11}C and ^{18}F labeled compounds,[37,38] also appears promising. However, information given by the radioligand approach relates to concentration of enzyme, whereas the metabolic trapping approach, which we have pursued can give information about flux through the enzyme. Other approaches to developing imaging agents for FAAH have involved substitutions at the −OH group of the ethanolamine moiety of acylethanolamines, and have not been encouraging.[9−11]

We would also note that use of the injection vehicle for the NAAA and control groups (Table 5, dimethyl sulfoxide/Cremophore/0.9% saline (20 μL/30 μL/150 μL) resulted 1.5−2.0 times higher uptake across brain regions. Due to the poor stability of the NAAA inhibitor, we chose not to administered the inhibitor Compound 7h intraperitoneally as done for URB-597. Instead, it was administered through a tail-vein, which precluded a second tail-vein injection. ^{18}F-FHEA was then administered retro-orbitally, which has become a commonly employed injection site in small animal PET studies. Thus, the higher brain uptake of ^{18}F-FHEA with Cremophore-containing vehicle could have resulted from enhanced blood-brain barrier penetration caused by the vehicle, or differences in the injection method.

■ CONCLUSION

An efficient synthesis of *N*-(16-^{18}F-fluorohexadecanoyl)-ethanolamine (^{18}F-FHEA) and nonradioactive standards has been achieved. The radiochromatographic experiments demonstrated that pretreatment of mice with URB-597 decreased conversion of ^{18}F-FHEA to free fatty acids and complex lipids. This is consistent with reports that URB-597 inhibits FAAH, an

dx.doi.org/10.1021/cn400214j | ACS Chem. Neurosci. 2014, 5, 793−802

Table 5. Uptake (% ID/g) and SUV of ^{18}F-FHEA in Swiss Webster Mice at 30 min Post-Injection Using NAAA Inhibitor[a]

tissue	%ID/g control (vehicle) mice	%ID/g NAAA inhibitor treated mice	%ID/g p-value[b]	SUV control (vehicle) mice	SUV NAAA inhibitor treated mice	SUV p-value[b]
cortex	8.87 ± 2.47	9.14 ± 1.63	0.8484	2.06 ± 0.57	2.11 ± 0.34	0.8748
cerebellum	9.05 ± 2.52	9.35 ± 1.80	0.8449	2.11 ± 0.59	2.15 ± 0.37	0.8850
brain stem	8.81 ± 2.48	9.46 ± 2.19	0.6912	2.05 ± 0.59	2.18 ± 0.46	0.7234
thalamus	8.42 ± 2.82	8.41 ± 1.99	0.9924	1.96 ± 0.66	1.94 ± 0.42	0.9508
hypothalamus	6.97 ± 2.12	8.06 ± 3.28	0.5906	1.62 ± 0.49	1.85 ± 0.71	0.6015
hippocampus	6.60 ± 1.51	7.73 ± 2.00	0.3899	1.53 ± 0.34	1.78 ± 0.42	0.3809
striatum	7.96 ± 1.83	8.24 ± 1.91	0.8349	1.85 ± 0.43	1.90 ± 0.41	0.8693
rest of brain	7.96 ± 1.91	8.24 ± 1.68	0.8210	1.85 ± 0.45	1.90 ± 0.35	0.8582
whole brain	8.21 ± 2.12	8.54 ± 1.80	0.8090	1.91 ± 0.50	1.97 ± 0.38	0.8554
blood	5.37 ± 1.05	5.42 ± 1.08	0.9492	1.25 ± 0.27	1.26 ± 0.27	0.9759
urine	59.03 ± 32.48	91.20 ± 97.27	0.5648	13.66 ± 7.32	21.06 ± 22.32	0.5635
heart	5.79 ± 2.28	4.65 ± 0.76	0.3381	1.35 ± 0.53	1.08 ± 0.18	0.3300
lung	14.00 ± 3.40	12.40 ± 4.99	0.6062	3.27 ± 0.83	2.88 ± 1.15	0.5913
liver	29.96 ± 3.84	26.75 ± 4.87	0.3250	6.98 ± 0.103	6.19 ± 1.09	0.3097
spleen	4.79 ± 1.14	4.47 ± 0.77	0.6404	1.12 ± 0.29	1.04 ± 0.18	0.6224
kidney	19.87 ± 5.66	19.48 ± 5.42	0.9189	4.64 ± 1.41	4.51 ± 1.22	0.8819
testis	2.05 ± 0.61	2.13 ± 0.41	0.8340	0.48 ± 0.15	0.49 ± 0.09	0.8712
fat	6.09 ± 3.06	2.88 ± 2.25	0.1133	1.42 ± 0.72	0.66 ± 0.52	0.1094
bone	5.09 ± 0.94	4.77 ± 0.90	0.6251	1.19 ± 0.24	1.10 ± 0.20	0.5949
muscle	1.87 ± 0.51	2.29 ± 0.88	0.4499	0.44 ± 0.13	0.53 ± 0.20	0.4685
skin	2.82 ± 0.74	3.00 ± 0.57	0.6971	0.66 ± 0.18	0.69 ± 0.12	0.7379

[a]Values are listed as mean ± standard deviation. There were 4 measurements for each time by body region category. [b]p-Value represents tests for differences in biodistribution across treatment groups. p-Values are not adjusted for multiple comparisons. [c]Statistically significant p-value.

enzyme that terminates signaling by the endocannabinoid anandamide, *N*-arachidonoylethanolamine. However, URB-597 did not significantly alter the brain regional concentration of ^{18}F-radioactivity after administration of ^{18}F-FHEA. Results with the NAAA inhibitor Compound 7h are inconclusive, although a predominant role of FAAH in ^{18}F-FHEA metabolism is implied by the large fraction of nonmetabolized ^{18}F-FHEA remaining in brain following URB-597 treatment. To conclude, ^{18}F-FHEA appears to behave as a good mimic of *N*-acylethanolamine uptake and FAAH-sensitive metabolism in brain but its utility as a PET probe of FAAH activity in the brain may be compromised by the lack of sensitivity of total cerebral ^{18}F-radioactivity concentration to changes in *N*-acylethanolamine hydrolysis rate.

METHODS

Materials and Methods. All chemicals and solvents were purchased from Sigma-Aldrich and used as received. Anhydrous solvents were also purchased from Sigma-Aldrich in "sure seal" bottles. TLC analysis of reaction mixtures and products was performed on Merck silica gel 60 F254 TLC plates. Liquid chromatography was carried out on Merck 60 silica gel (32−63 μm). ^{1}H and ^{13}C NMR was recorded on a Varian 600 MHz spectrometer. Mass spectral data were obtained from the Mass Spectral Lab of School of Chemical Sciences, University of Illinois, Urbana, Illinois. Analytical HPLC was performed on a Phenomenex Luna C-18 column (5 μm, 4.6 × 250 mm) with a flow rate of 0.8 mL/min. Semipreparative HPLC was performed on the final ^{18}F-labeled product using a Phenomenex Luna C-18 column (5 μm, 10 × 250 mm) with a flow rate of 5.0 mL/min using 80:20 acetonitrile/water as an eluent at 220 nm UV wavelength. URB 597 was purchased from Merck Chemicals.

General Procedure for ^{18}F-Labeling. For ^{18}F-labeling, cyclotron-produced ^{18}F-fluoride (20 mCi) was dried down under nitrogen at 95 °C in a 3 mL glass vial containing Kryptofix 2.2.2 (10 mg), acetonitrile (0.8 mL), and K_2CO_3 (4 mg) solution in water (0.50 mL). The residue was further dried by azeotropic distillation with anhydrous acetonitrile (3 × 0.5 mL). The ^{18}F-fluoride residue was reconstituted in 0.5 mL of acetonitrile, and the bromo precursor (approximately 2−3 mg) in acetonitrile (0.5 mL) was added. The resultant reaction mixture was heated with a PETWave microwave reactor for 10 min at 80 °C. ^{18}F-fluoride incorporation was checked using silica-gel r-TLC (8:92 methanol/chloroform). Deprotection was carried out by addition of 0.45 mL of 15%TFA aqueous solution followed by heating in the microwave reactor for 5 min at 60 °C. After deprotection, the crude product was purified by using a semi-preparative C-18 HPLC (80:20 ACN/H_2O) system. The product peak was collected at 7.3 min retention time with >99% radiochemical purity, which was in complete agreement with the cold standard. The product peak was diluted in water, concentrated on a C-18 Sep-Pak column, and eluted in 1 mL of ethanol. The specific activity of the final product was found to be in the range of 1.4−5.1 Ci/μmol. Final product was formulated in 0.5−1% BSA in isotonic NaCl solution and filtered through a 0.22 μm filter before being administered to mice.

Biodistribution Method. Swiss Webster mice (body wt 24−28 g) were used in this study under approval of Institutional Animal Care and Use Committees (IACUCs) of Northeastern University and Mayo Clinic. The mice were anesthetized with isoflurane (3.0% induction, 2.0−2.5% maintenance) for imaging studies. For biodistribution studies, conscious mice were intravenously injected with 200 μL of ^{18}F-FHEA (0.37−0.74 MBq) formulated in 0.5−1% BSA in isotonic NaCl solution and filtered through a 0.22 μm filter (Millex-GS, Millipore, Bedford, MA). Radiochemical purity (>99%) was analyzed by radio-HPLC as described above. After 1−60 min administration, the animals were euthanized by cervical dislocation, and the brains dissected on a moist filter paper using forceps. Brain regions hypothalamus, olfactory tubercles, striatum, hippocampus, cerebellum, brain stem, cortex, thalamus, and rest-of-brain were rapidly weighed and then assayed for ^{18}F-radioactivity, together with injection standards, whereas rest-of-body biodistribution was performed by procurement of heart, liver, lung, spleen, kidney, testis, fat, skin, bone (femur) blood, urine, and skeletal muscle. Another set of Swiss Webster mice was used to examine the effect of FAAH inhibitor URB 597 on uptake and biodistribution of ^{18}F-FHEA. For this, animals were pretreated with 1 mg/kg of URB 597 dissolved in 75% DMSO solution and injected intraperitoneally 60 min prior to the ^{18}F-FHEA injection. The synthesized NAAA inhibitor is formulated in dimethyl

sulfoxide/Cremephore/0.9% saline (20 μL/30 μL/150 μL) solutions. Each injection was 200 μL having 0.75 mg of NAAA inhibitor (Compound 7h). The tissues were counted for ^{18}F-radioactivity and weighed. All ^{18}F-radioactivity measurements were corrected for radioactivity decay.

Following correction for background and physical decay, data were expressed as a percent of injected activity per gram of wet weight (% ID/g) and SUV (standard uptake value) using eqs 1 and 2, respectively.

$$\%\frac{\mathrm{ID}}{\mathrm{g}} = \frac{\mathrm{At}}{W_\mathrm{t}}\frac{1}{D_\mathrm{inj}} \times 100\ (\%/g) \tag{1}$$

where At = tissue activity, W_t = tissue weight, D_{inj} = dose injected.

$$\mathrm{SUV} = \left(\%\frac{\mathrm{ID}}{g}\right)W_\mathrm{a}/100 \tag{2}$$

where W_a = animal weight

Metabolite Analysis. Analysis of the metabolic fate of ^{18}F-FHEA in the brain was performed by using a Folch-type extraction procedure as described in literature.[19,21] Approximately 0.05 g of cerebellum was excised and thoroughly homogenized and sonicated (20 s) in 2.4 mL of chloroform/methanol (2:1) at 0 °C. Urea (40%, 0.6 mL) and 5% sulfuric acid (0.6 mL) were added, and the mixture was sonicated for an additional 20 s. After centrifugation for 10 min at 1800 rpm, aqueous and organic fractions were separated and counted for radioactivity. Organic fraction was concentrated under nitrogen and subjected on radio-thin layer chromatographic (r-TLC) studies. Silica coated glass TLC plate and petroleum ether/diethyl ether/acetic acid as (v/v) 70:30:1 as mobile phase were used for the analysis of the metabolites formed after 5 min of injection of ^{18}F-FHEA. Cyclone Plus Phosphor Imager by PerkinElmer was used to analyze the r-TLC plate.

We did not include the radioactivity associated with the protein pellet in this study. In pilot studies using [arachidonoyl-^{14}C]-anandamide, this fraction represented <10% of total radioactivity without further extraction of the pellet. The obtained mean activity distributions were (n = 4) organic or chloroform layer = 89.2%, aqueous layer = 1.3%, and protein pellet = 9.5%.

Measurement of IC_{50} for Inhibition of Anandamide Hydrolysis in Mouse Brain Homogenate. Mouse forebrain homogenates (n = 4) were prepared using a Polytron-type homogenizer and ice-cold buffer (10 mL) as previously described.[39] The buffer was tris/magnesium chloride/EDTA (100/5/1 in mM) containing 2.5% bovine serum albumin. To 0.1 mL of buffer containing [ethanolamine-^{14}C]anandamide (10 nCi/tube) and non-radioactive *N*-acylethanolamines (100−600 μM) was added 0.1 mL of pooled brain homogenates (equivalent of ∼0.5 mg of brain wet weight), and incubated at 25 °C for 10 min. The reactions were terminated by addition of 0.5 mL of 2 N HCl and 0.5 mL of chloroform. After vortexing and centrifuging the sample, 0.25 mL of the acid layer was removed for liquid scintillation counting. Since the anandamide substrate concentration (2 μM) used in the assays was much lower than the inhibitor concentrations, IC_{50} values were determined on the basis of the equation:

$$\mathrm{IC}_{50} = C_\mathrm{i}\mathrm{CPM}_\mathrm{i}/(\mathrm{CPM}_\mathrm{c} - \mathrm{CPM}_\mathrm{i}) \tag{3}$$

where C_i is the inhibitor concentration, CPM_i is count rate in the presence of inhibitor, and CPM_c is control count rate in the absence of inhibitor.

Statistical Analysis. Results are expressed as mean ± SD. Mean values were compared by using repeated measures ANOVA in SAS PROC Mixed (SAS/STAT version 12.1, Cary, NC). This analysis accounted for the repeated measurements within animal and the between subject effect of either time or treatment. Reported p-values have not been adjusted for multiple comparisons. Fisher's least significant difference was used to control the overall experiment-wise error rate, and as such $p < 0.05$ was interpreted as statistically significant only if the overall model was statistically significant, which was the case for the data presented in Tables 1−4.

Synthesis of *N*-(16-Bromohexadecanoyl)ethanolamine (1). Synthesis of *N*-(16-bromohexadecanoyl)ethanolamine (**1**) was achieved by stirring of 16-bromo hexadecanoic acid (2.00 g, 5.97 mmol), methyl chloroformate (1.128 g, 11.94 mmol), and triethylamine (1.204 g, 11.94 mmol) in dichloromethane at 0 °C for 30 min and then at room temperature for another 1.5 h. After 2 h, reaction temperature was further lowered to 0 °C for addition of ethanolamine (0.728 g, 11.94 mmol), and the resultant reaction mixture was stirred at room temperature overnight. After completion, solvent was removed under vacuum and cold water was poured into the flask containing residue with constant stirring for additional 10 min. Solid obtained was filtered and dried. TLC was re-examined for desired product in 8:92 methanol/chloroform as a solvent system. The residue was subjected to column chromatography using silica gel as an adsorbent and 5:95 methanol/chloroform as solvent to yield compound **1** (1.96 g, 87% yield, mp 90 ± 1 °C) as a white solid. ^{1}H NMR (25 °C, 599.77 MHz, $CDCl_3$) δ ppm: 5.88 (brs, 1H, NH), 3.66 (t, 2H, $J_{1,2}$ = 6.0 Hz, CH_2), 3.34 (m, 4H, 2 × CH_2), 2.14 (t, 2H, J = 6.0 Hz, CH_2), 1.78 (m, 2H, CH_2), 1.56 (m, 2H, CH_2), 1.35 (m, 2H, CH_2), 1.23−1.18 (brs, 20H, 10 ×CH_2). ^{13}C NMR (25 °C, 150.81 MHz, $CDCl_3$) δ ppm: 177.2 (CONH), 65.3 (CH_2OH), 45.1, 39.3, 36.7, 35.4, 32.3−31.9 (CH_2 × 9), 31.4, 30.8, 28.3. HRMS (ES) calcd for $C_{18}H_{36}O_2NBr$ (M^+), 377.19293; found, 377.19241 and (M+2) at 379.1 (due to isotopic abundance).

Synthesis of 16-Bromo-*N*-[2[(tetrahydro-2*H*-pyran-2-yl)oxy]-ethyl]hexadecanoylamide (2). Synthesis of 16-bromo-*N*-[2-[(tetrahydro-2*H*-pyran-2-yl)oxy]ethyl]hexadecanoylamide (**2**) was achieved by stirring of *N*-(16-bromohexadecanoyl)ethanolamine (**1**) (1.00 g, 2.65 mmol), 3,4-dihydro-2*H*-pyran (0.29 g, 3.44 mmol) in dichloromethane using *p*-toluenesulfonic acid as catalyst (0.548 g, 3.18 mmol). The mixture was stirred for 24 h at room temperature and quenched with water. After extraction with the chloroform, organic layer was dried over Na_2SO_4 and solvent was evaporated under vacuum. The residue was subjected to column chromatography (2:98 methanol: chloroform) to yield **2** (0.93 g, 76% yield, mp 60 ± 1 °C) as a white solid. ^{1}H NMR (25 °C, 599.77 MHz, $CDCl_3$) δ ppm: 6.00 (brs, 1H, NH), 4.55 (t, 1H), 3.88 (m, 1H), 3.76 (m, 1H), 3.61 (m, 1H), 3.55 (m, 1H), 3.47 (m, 2H), 3.41 (t, 2H, $J_{1,2}$ = 6.0 Hz, CH_2Br), 2.17 (t, 2H, J = 6.0 Hz, CH_2), 1.86 (m, 2H, CH_2), 1.62 (m, 2H, CH_2), 1.53 (m, 2H, CH_2), 1.41 (m, 2H, CH_2), 1.29−1.25 (brs, 24H, 12× CH_2). ^{13}C NMR (25 °C, 150.81 MHz, $CDCl_3$) δ ppm: 173.1 (CONH), 99.7 (OCHO), 67.1, 63.2, 39.4, 36.8, 34.0, 32.8, 30.7, 29.6−29.3 (CH_2 × 9), 28.7, 28.1, 25.7, 25.2, 20.0. HRMS (ES) calcd for $C_{23}H_{44}O_3NBr$ (M^+), 461.24263; found, 461.24182 and (M+2) at 463.3 (due to isotopic abundance).

Synthesis of *N*-(16-Fluorohexadecanoyl)ethanolamine (3). Synthesis of *N*-(16-fluorohexadecanoyl)ethanolamine (**3**) was achieved by stirring 16-bromo-*N*-[2[(tetrahydro-2*H*-pyran-2-yl)oxy]-ethyl]hexadecanoylamide (**2**) (0.50 g, 1.08 mmol) and 1 M THF solution tetra-*n*-butylammonium fluoride (1.2 mL) in acetonitrile. The resulting solution was stirred for 72 h at room temperature with two subsequent additions of 0.5 mL of 1 M tetra-*n*-butylammonium fluoride in THF after 24 and 48 h. TLC was used to monitor the progress of reaction; after completion, solvent was removed under vacuum. The obtained residue was dissolved in methanol with few drops of water, a catalytic amount of *p*-toluenesulfonic acid (100 mg, 0.58 mmol) was added, and the mixture was stirred for 2 h at room temperature. After 2 h, TLC was re-examined for deprotection of tetrahydropyranyl group. Subsequently, solvent was removed under vacuum and residue was extracted against water in dichloromethane. Thereafter, the organic layer was dried over Na_2SO_4, and solvent was evaporated under vacuum. The obtained residue was subjected to column chromatography (5:95 methanol/chloroform) to yield compound **3** (0.175g, 51% yield, mp 97 ± 1 °C) as a white solid. ^{1}H NMR (25 °C, 399.62 MHz, $CDCl_3$) δ ppm: 5.87 (brs, 1H, NH), 4.43−4.31 (dt, 2H, J_1 = 48.0 Hz, J_2 = 6.0 Hz, CH_2F), 3.66 (t, 2H, $J_{1,2}$ = 4.0 Hz CH_2OH), 3.36 (m, 2H, CH_2NH), 2.64 (brs, 1H, OH), 2.13 (m, 2H), 1.65 (m, 2H, CH_2), 1.57 (m, 2H, CH_2), 1.31 (m, 2H, CH_2), 1.28−1.19 (brs, 20H, 10 × CH_2). ^{13}C NMR (25 °C, 100.48 MHz, $CDCl_3$) δ ppm: 174.5 (CONH), 85.0−83.4 (d, J = 160 Hz, **C**H_2F),

dx.doi.org/10.1021/cn400214j | ACS Chem. Neurosci. 2014, 5, 793−802

62.6, 42.4, 36.6, 30.4, 30.2, 29.6−29.3 (CH_2 × 10), 25.7, 25.2−25.0 (d, J = 20 Hz). ^{19}F NMR (25 °C, 376.02 MHz, $CDCl_3$) δ ppm: −218 (m, 1F, CH_2**F**). HRMS (ES) calcd for $C_{18}H_{36}O_2NF$ (M^+), 317.27300; found, 317.27254.

■ ASSOCIATED CONTENT

Supporting Information

Synthesis of nonradioactive standards and their spectrascopic characterization, radio-TLC of compounds 4 and 8, and micro-PET images of 18F-FHEA in mice. This material is available free of charge via the Internet at http://pubs.acs.org.

■ AUTHOR INFORMATION

Corresponding Authors

*E-mail: degrado.timothy@mayo.edu. Phone: 507-538-4319. Fax 507-293-2235.

*E-mail: s.gatley@neu.edu. Phone: 617.373.3306. Fax: 617-373-8886.

Author Contributions

M.K.P. performed the synthesis, purification, and chemical characterization of compounds **1**−**8** and NAAA inhibitor. M.K.P and T.R.D. developed the initial radiosynthesis, whereas M.K.P and M.S.J. did the microwave-assisted automation of the radiosynthesis using TRACERLab FXN Pro synthetic module and routinely produced the tracer for biological evaluations. J.S.G., T.R.D., and M.K.P. did the biological evaluation in Swiss Webster mice. K.Q., J.S.G., and R.I.D. performed TLC of nonradioactive standards of various lipids and also performed the competitive inhibition measurements. Statistical analysis was carried out by C.E.H., T.R.D., and M.K.P. The manuscript was prepared by M.K.P and edited by T.R.D., J.S.G., and R.I.D. All authors have given approval to the final version of the manuscript.

Funding

Present work was financially supported by the Department of Energy, Office of Science, DER, Biological and Environmental Research Grant to J.S.G. (DE SC0005251) and Mayo Clinic's "Radiology Advance Award" to M.K.P. and T.R.D.

Notes

The authors declare no competing financial interest.

■ ABBREVIATIONS

CB, cannabinoid; FAAH, fatty acid amide hydrolase; CB1/2, cannabinoid receptor1/2; ^{18}F-FHEA, *N*-(16-^{18}F-fluorohexadecanoyl)ethanolamine; URB-597, FAAH inhibitor, [3-(3-carbamoylphenyl)phenyl] *N*-cyclohexylcarbamate, also known as KDS-4103; MBq, megabecquerel; DMSO, dimethyl sulfoxide; ACN, acetonitrile; DCM, dichloromethane; *p*-TsCl, *p*-toluene sulfonyl chloride; DHP, dihydropyran; TBAF, *n*-butylammoniumfluoride; TFA, trifluoroacetic acid; *p*-TSA, *p*-toluene sulfonic acid; K2.2.2, Kryptofix chemically known as 4,7,13,16,21,24-hexaoxa-1,10-diazabicyclo[8.8.8]hexacosane; anandamide, also known as *N*-arachidonoylethanolamine, AEA, an endogenous cannabinoid neurotransmitter; TLC, thin layer chromatography; r-TLC, radioactive thin layer chromatography; IACUC, Institutional Animal Care and Use Committee; PETwave Microwave, a microwave unit produced by CEM corporation; TRACERLab FXN Pro, a radiosynthetic module produced by General Electric Healthcare; PET, positron emission tomography; NAAA, *N*-acylethanolamine-hydrolyzing acid amidase; SPECT, single photon emission computed tomography; IC_{50}, half-maximal inhibitory concentration

■ REFERENCES

(1) Hillard, C. J., Weinlander, K. M., and Stuhr, K. L. (2012) Contributions of endocannabinoid signaling to psychiatric disorders in humans: Genetic and biochemical evidence. *Neuroscience 204*, 207−229.

(2) Hill, M. N., Patel, S., Campolongo, P., Tasker, J. G., Wotjak, C. T., and Bains, J. S. (2010) Functional interactions between stress and the endocannabinoid system: From synaptic signaling to behavioral output. *J. Neurosci. 30*, 14980−14986.

(3) Di Marzo, V., Ligresti, A., and Cristino, L. (2009) The endocannabinoid system as a link between homoeostatic and hedonic pathways involved in energy balance regulation. *Int. J. Obes. 33*, S18−S24.

(4) Pacher, P., and Mechoulam, R. (2011) Is lipid signaling through cannabinoid 2 receptors part of a protective system? *Prog. Lipid Res. 50*, 193−211.

(5) Hill, M. N., Kumar, S. A., Filipski, S. B., Iverson, M., Stuhr, K. L., Keith, J. M., Cravatt, B. F., Hillard, C. J., Chattarji, S., and McEwen, B. S. (2013) Disruption of fatty acid amide hydrolase activity prevents the effects of chronic stress on anxiety and amygdalar microstructure. *Mol. Psychiatry 18*, 1125−1135.

(6) Conzelmann, A., Reif, A., Jacob, C., Weyers, P., Lesch, K. P., Lutz, B., and Pauli, P. (2012) A polymorphism in the gene of the endocannabinoid-degrading enzyme FAAH (FAAH C385A) is associated with emotional-motivational reactivity. *Psychopharmacology (Berlin, Ger.) 224*, 573−579.

(7) Choi, K., Le, T., McGuire, J., Xing, G., Zhang, L., Li, H., Parker, C. C., Johnson, L. R., and Ursano, R. J. (2012) Expression pattern of the cannabinoid receptor genes in the frontal cortex of mood disorder patients and mice selectively bred for high and low fear. *J. Psychiatr. Res. 46*, 882−889.

(8) Monteleone, P., Bifulco, M., Maina, G., Tortorella, A., Gazzerro, P., Proto, M. C., Di Filippo, C., Monteleone, F., Canestrelli, B., Buonerba, G., Bogetto, F., and Maj, M. (2010) Investigation of CNR1 and FAAH endocannabinoid gene polymorphisms in bipolar disorder and major depression. *Pharmacol. Res. 61*, 400−404.

(9) Wyffels, L., De Bruyne, S., Blanckaert, P., Lambert, D. M., and De Vos, F. (2009) Radiosynthesis, in vitro and in vivo evaluation of ^{123}I-labeled anandamide analogues for mapping brain faah. *Bioorg. Med. Chem. 17*, 49−56.

(10) Wyffels, L., Muccioli, G. G., De Bruyne, S., Moerman, L., Sambre, J., Lambert, D. M., and De Vos, F. (2009) Synthesis, in vitro and in vivo evaluation, and radiolabeling of aryl anandamide analogues as candidate radioligands for in vivo imaging of fatty acid amide hydrolase in the brain. *J. Med. Chem. 52*, 4613−4622.

(11) Wyffels, L., Muccioli, G. G., Kapanda, C. N., Labar, G., De Bruyne, S., De Vos, F., and Lambert, D. M. (2010) PET imaging of fatty acid amide hydrolase in the brain: Synthesis and biological evaluation of an ^{11}C-labelled URB597 analogue. *Nucl. Med. Biol. 37*, 665−675.

(12) Glaser, S. T., Gatley, S. J., and Gifford, A. N. (2006) Ex vivo imaging of fatty acid amide hydrolase activity and its inhibition in the mouse brain. *J. Pharmacol. Exp. Ther. 316*, 1088−1097.

(13) Wilson, A. A., Garcia, A., Parkes, J., Houle, S., Tong, J., and Vasdev, N. (2011) [^{11}C]CURB: Evaluation of a novel radiotracer for imaging fatty acid amide hydrolase by positron emission tomography. *Nucl. Med. Biol. 38*, 247−253.

(14) Sun, Y. X., Tsuboi, K., Zhao, L. Y., Okamoto, Y., Lambert, D. M., and Ueda, N. (2005) Involvement of *N*-acylethanolamine-hydrolyzing acid amidase in the degradation of anandamide and other *N*-acylethanolamines in macrophages. *Biochim. Biophys. Acta 1736*, 211−220.

(15) Ueda, N., Tsuboi, K., and Uyama, T. (2010) *N*-acylethanolamine metabolism with special reference to *N*-acylethanolamine-hydrolyzing acid amidase (NAAA). *Prog. Lipid Res. 49*, 299−315.

(16) Ueda, N., Tsuboi, K., and Uyama, T. (2013) Metabolism of endocannabinoids and related *N*-acylethanolamines: Canonical and alternative pathways. *FEBS J. 280*, 1874−1894.

(17) Tsuboi, K., Takezaki, N., and Ueda, N. (2007) The *N*-acylethanolamine-hydrolyzing acid amidase (NAAA). *Chem. Biodiversity 4*, 1914−1925.
(18) Snider, N. T., Walker, V. J., and Hollenberg, P. F. (2010) Oxidation of the endogenous cannabinoid arachidonoyl ethanolamide by the cytochrome P450 monooxygenases: Physiological and pharmacological implications. *Pharmacol. Rev. 62*, 136−154.
(19) Ueda, N., Puffenbarger, R. A., Yamamoto, S., and Deutsch, D. G. (2000) The fatty acid amide hydrolase (FAAH). *Chem. Phys. Lipids 108*, 107−121.
(20) McKinney, M. K., and Cravatt, B. F. (2005) Structure and function of fatty acid amide hydrolase. *Annu. Rev. Biochem. 74*, 411−432.
(21) Fowler, C. J., Borjesson, M., and Tiger, G. (2000) Differences in the pharmacological properties of rat and chicken brain fatty acid amidohydrolase. *Br. J. Pharmacol. 131*, 498−504.
(22) Tsuboi, K., Sun, Y. X., Okamoto, Y., Araki, N., Tonai, T., and Ueda, N. (2005) Molecular characterization of *N*-acylethanolamine-hydrolyzing acid amidase, a novel member of the choloylglycine hydrolase family with structural and functional similarity to acid ceramidase. *J. Biol. Chem. 280*, 11082−11092.
(23) Jonsson, K. O., Vandevoorde, S., Lambert, D. M., Tiger, G., and Fowler, C. J. (2001) Effects of homologues and analogues of palmitoylethanolamide upon the inactivation of the endocannabinoid anandamide. *Br. J. Pharmacol. 133*, 1263−1275.
(24) Ho, W. S. V., Barrett, D. A., and Randall, M. D. (2008) "Entourage" effects of *N*-palmitoylethanolamide and *N*-oleoylethanolamide on vasorelaxation to anandamide occur through trpv1 receptors. *Br. J. Pharmacol. 155*, 837−846.
(25) O'Sullivan, S. E. (2007) Cannabinoids go nuclear: Evidence for activation of peroxisome proliferator-activated receptors. *Br. J. Pharmacol. 152*, 576−582.
(26) Lo Verme, J., Fu, J., Astarita, G., La Rana, G., Russo, R., Calignano, A., and Piomelli, D. (2005) The nuclear receptor peroxisome proliferator-activated receptor-alpha mediates the anti-inflammatory actions of palmitoylethanolamide. *Mol. Pharmacol. 67*, 15−19.
(27) Guan, L. P., Zhao, D. H., Xiu, J. H., Sui, X., Piao, H. R., and Quan, Z. S. (2009) Synthesis and anticonvulsant activity of *N*-(2-hydroxyethyl)amide derivatives. *Arch. Pharm. 342*, 34−40.
(28) Pandey, M. K., Belanger, A. P., Wang, S., and DeGrado, T. R. (2012) Structure dependence of long-chain [^{18}F]fluorothia fatty acids as myocardial fatty acid oxidation probes. *J. Med. Chem. 55*, 10674−10684.
(29) Belanger, A. P., Pandey, M. K., and DeGrado, T. R. (2011) Microwave-assisted radiosynthesis of [^{18}F]fluorinated fatty acid analogs. *Nucl. Med. Biol. 38*, 435−41.
(30) Solorzano, C., Antonietti, F., Duranti, A., Tontini, A., Rivara, S., Lodola, A., Vacondio, F., Tarzia, G., Piomelli, D., and Mor, M. (2010) Synthesis and structure-activity relationships of *N*-(2-oxo-3-oxetanyl)-amides as *N*-acylethanolamine-hydrolyzing acid amidase inhibitors. *J. Med. Chem. 53*, 5770−5781.
(31) Duranti, A., Tontini, A., Antonietti, F., Vacondio, F., Fioni, A., Silva, C., Lodola, A., Rivara, S., Solorzano, C., Piomelli, D., Tarzia, G., and Mor, M. (2012) *N*-(2-oxo-3-oxetanyl)carbamic acid esters as *N*-acylethanolamine acid amidase inhibitors: Synthesis and structure-activity and structure-property relationships. *J. Med. Chem. 55*, 4824−4836.
(32) DeGrado, T. R., Bhattacharyya, F., Pandey, M. K., Belanger, A. P., and Wang, S. (2010) Synthesis and preliminary evaluation of 18-[^{18}F]-fluoro-4-thia-oleate as a pet probe of fatty acid oxidation. *J. Nucl. Med. 51*, 1310−1317.
(33) Rapoport, S. I. (2005) In vivo approaches and rationale for quantifying kinetics and imaging brain lipid metabolic pathways. *Prostaglandins Other Lipid Mediators 77* (1−4), 185−96.
(34) Tai, T., Tsuboi, K., Uyama, T., Masuda, K., Cravatt, B. F., Houchi, H., and Ueda, N. (2012) Endogenous molecules stimulating *N*-acylethanolamine-hydrolyzing acid amidase (NAAA). *ACS Chem. Neurosci. 3* (5), 379−85.
(35) Kaczocha, M., Rebecchi, M. J., Ralph, B. P., Teng, Y. H., Berger, W. T., Galbavy, W., Elmes, M. W., Glaser, S. T., Wang, L., Rizzo, R. C., Deutsch, D. G., and Ojima, I. (2014) Inhibition of Fatty Acid binding proteins elevates brain anandamide levels and produces analgesia. *PLoS One 9* (4), e94200.
(36) Fowler, C. J. (2013) Transport of endocannabinoids across the plasma membrane and within the cell. *FEBS J. 280* (9), 1895−904.
(37) Sadovski, O., Hicks, J. W., Parkes, J., Raymond, R., Nobrega, J., Houle, S., Cipriano, M., Fowler, C. J., Vasdev, N., and Wilson, A. A. (2013) Development and characterization of a promising fluorine-18 labelled radiopharmaceutical for in vivo imaging of fatty acid amide hydrolase. *Bioorg. Med. Chem. 21* (14), 4351−7.
(38) Hicks, J. W., Parkes, J., Sadovski, O., Tong, J., Houle, S., Vasdev, N., and Wilson, A. A. (2013) Synthesis and preclinical evaluation of [^{11}C-carbonyl] PF-04457845 for neuroimaging of fatty acid amide hydrolase. *Nucl. Med. Biol. 40* (6), 740−746.
(39) Omeir, R. L., Chin, S., Hong, Y., Ahern, D. G., and Deutsch, D. G. (1995) Arachidonoyl ethanolamide-[1, 2-^{14}C] as a substrate for anandamide amidase. *Life Sci. 56* (23/24), 1999−2005.